Plasma fibronectin stabilizes *Borrelia burgdorferi*–endothelial interactions under vascular shear stress by a catch-bond mechanism

Alexandra F. Niddam[a], Rhodaba Ebady[a], Anil Bansal[a], Anne Koehler[a], Boris Hinz[a], and Tara J. Moriarty[a,b,1]

[a]Matrix Dynamics Group, Faculty of Dentistry, University of Toronto, Toronto, ON, Canada M5S 3E2; and [b]Laboratory Medicine & Pathobiology, Matrix Dynamics Group, Faculty of Medicine, University of Toronto, Toronto, ON, Canada M5S 3E2

Edited by Lalita Ramakrishnan, University of Cambridge, Cambridge, United Kingdom, and approved March 7, 2017 (received for review September 7, 2016)

Bacterial dissemination via the cardiovascular system is the most common cause of infection mortality. A key step in dissemination is bacterial interaction with endothelia lining blood vessels, which is physically challenging because of the shear stress generated by blood flow. Association of host cells such as leukocytes and platelets with endothelia under vascular shear stress requires mechanically specialized interaction mechanisms, including force-strengthened catch bonds. However, the biomechanical mechanisms supporting vascular interactions of most bacterial pathogens are undefined. Fibronectin (Fn), a ubiquitous host molecule targeted by many pathogens, promotes vascular interactions of the Lyme disease spirochete *Borrelia burgdorferi*. Here, we investigated how *B. burgdorferi* exploits Fn to interact with endothelia under physiological shear stress, using recently developed live cell imaging and particle-tracking methods for studying bacterial–endothelial interaction biomechanics. We found that *B. burgdorferi* does not primarily target insoluble matrix Fn deposited on endothelial surfaces but, instead, recruits and induces polymerization of soluble plasma Fn (pFn), an abundant protein in blood plasma that is normally soluble and nonadhesive. Under physiological shear stress, caps of polymerized pFn at bacterial poles formed part of mechanically loaded adhesion complexes, and pFn strengthened and stabilized interactions by a catch-bond mechanism. These results show that *B. burgdorferi* can transform a ubiquitous but normally nonadhesive blood constituent to increase the efficiency, strength, and stability of bacterial interactions with vascular surfaces. Similar mechanisms may promote dissemination of other Fn-binding pathogens.

catch bond | fibronectin | force | vascular | bacteria

Dissemination of pathogens via the cardiovascular system is associated with most mortality due to bacterial infection, and is important for infection of many tissues, including the brain, heart, bone, joints, and visceral organs (1). Pathogens that travel via the cardiovascular system to sites distant from the original source of infection must be able to adhere to the inner endothelial lining of blood vessels to slow down and migrate out of the vasculature (extravasate) into extravascular tissues. Other pathogens do not exit the bloodstream, but can adhere tenaciously to structures such as heart valves and cardiac devices, causing life-threatening conditions, including endocarditis (2). Despite the importance of pathogen vascular adhesion and dissemination to human health, the mechanisms supporting these processes are largely uncharacterized for many microbes, including most bacterial pathogens.

The ability to overcome fluid shear stress caused by blood flow over endothelial surfaces is crucial for pathogens interacting with blood vessels. In the vasculature, interactions of circulating host cells such as leukocytes with endothelia are also subjected to fluid shear stress, and are stabilized by specialized force-resisting and force-strengthened mechanisms such as catch bonds and tethers (3, 4). Shock-absorbing structures such as pili and fimbriae can stabilize surface adhesion of bacteria subjected to external forces such as shear stress (5, 6). However, many bacteria, including spirochetes, do not form pili or fimbriae. We recently found that endothelial interactions of the Lyme disease spirochete *Borrelia burgdorferi* under physiological shear stress bear a remarkable biomechanical resemblance to the mechanisms supporting leukocyte rolling on the same surfaces and are stabilized by catch bonds and tethers, even though leukocytes and *B. burgdorferi* are genetically, morphologically, and physiologically distinct cells (7). Other bacterial pathogens also exploit or mimic strategies used by circulating host cells to adhere to and bypass endothelial barriers under vascular shear stress. For example, *Neisseria meningitidis* bypasses the blood–brain barrier by eliciting inflammatory responses and associated reorganization of brain endothelia following adhesion to a matrix metalloprotease regulator (8), and *Staphylococcus aureus* adheres to blood vessels walls by binding to fibrils of von Willebrand factor, a glycoprotein produced by endothelial cells that is crucial for adhesion of circulating platelets (9, 10). Thus, it appears that bacterial exploitation of ubiquitous host cell molecules and mimicry of common host cell shear-stress adhesion mechanisms are important for pathogen dissemination in this specialized and physically challenging environment.

One of the most abundant proteins in the cardiovascular system is fibronectin (Fn), which is part of the fibrous extracellular matrix supporting endothelial cells, and is also present in soluble form at high concentrations in blood [plasma Fn (pFn)] (11, 12). Fn interacts with integrins by a force-strengthened catch-bond mechanism, and Fn and integrins can mediate leukocyte adhesion

Significance

Spread of bacteria via the bloodstream to vital organs causes most mortality due to bacterial infection. To exit the bloodstream and enter these organs, bacteria must be able to resist the forces generated by flowing blood so that they can adhere to the endothelial cells lining blood vessels without being washed away. This process is not yet understood for most disease-causing bacteria. Here, we show that the Lyme disease pathogen *Borrelia burgdorferi* exploits an abundant constituent of blood, plasma fibronectin, to form endothelial interactions that become stronger as forces due to blood-flow increase. The ability to recruit this highly conserved molecule may also be important for the vascular interaction mechanisms of other pathogens.

Author contributions: A.B. and T.J.M. designed research; A.F.N., R.E., A.B., A.K., and T.J.M. performed research; A.F.N., A.B., and T.J.M. contributed new reagents/analytic tools; A.F.N., R.E., A.B., and T.J.M. analyzed data; A.F.N., R.E., A.K., B.H., and T.J.M. wrote the paper; and B.H. and T.J.M. supervised the project.

The authors declare no conflict of interest.

This article is a PNAS Direct Submission.

Freely available online through the PNAS open access option.

[1]To whom correspondence should be addressed. Email: tara.moriarty@utoronto.ca.

This article contains supporting information online at www.pnas.org/lookup/suppl/doi:10.1073/pnas.1615007114/-/DCSupplemental.

to vascular surfaces under physiological shear stress (13–17). Therefore, Fn has the potential to support vascular interactions of disseminating pathogens. Consistent with this hypothesis, *B. burgdorferi* interacts with postcapillary venules (PCVs) in vivo by an Fn-dependent mechanism (7, 18, 19), and polymorphisms in an *S. aureus* adhesion protein (adhesin) that strengthen Fn binding are associated with infection of cardiac devices by these bacteria (20). Fn-binding sequences of the surface-localized *B. burgdorferi* vascular adhesin BBK32 are also important for PCV interactions of this pathogen (19).

Most invasive bacterial pathogens that infect vertebrates target Fn and can adhere to this highly conserved molecule via bacterial cell surface adhesion proteins (adhesins) collectively referred to as bacterial Fn-binding proteins (FnBPs) (12, 21, 22). FnBPs can adhere to the insoluble Fn matrix and soluble unpolymerized Fn produced by most host cells, and many FnBPs also bind pFn, which is produced by the liver and is important for hemostasis and wound healing in vertebrates (23, 24). The ability of bacterial pathogens to recruit soluble Fn to their surfaces can promote adhesion to and internalization by host cells, as well as bacterial aggregation during biofilm formation (12, 22). However, the specific pathogenic functions of bacterial pFn binding have not yet been defined.

We reported recently that the Fn-binding *B. burgdorferi* vascular adhesin BBK32 stabilizes bacterial–endothelial interactions at PCV shear stress by a catch-bond mechanism (7). BBK32, which binds to Fn by a mechanism similar to the binding mechanisms of *S. aureus* FnBPA and streptococcal FnBPs (21, 25), causes conformational changes in pFn that induce formation of an extended structure (26) and formation of superfibronectin, a highly cross-linked, exceptionally sticky, polymerized form of Fn (27, 28). Several other pathogens and FnBPs adhere to Fn under force conditions similar to the force conditions found in the vasculature, suggesting that the use of Fn for vascular adhesion may be widespread among microbes (29–32). The mechanisms by which Fn promotes bacterial interactions with surfaces in the cardiovascular system have not yet been defined.

Here, we investigated how Fn promotes *B. burgdorferi*-endothelial interactions, using a recently developed flow chamber system that reproduces *B. burgdorferi*–endothelial interaction properties in PCVs and real-time live cell imaging and particle tracking approaches for studying interaction biomechanics. We found that *B. burgdorferi*–endothelial interactions are dependent on bacterial recruitment of pFn, which forms polymerized Fn sheaths at bacterial ends that are part of mechanical load-bearing adhesion complexes in BBK32-expressing bacteria, and that pFn stabilizes BBK32-mediated interactions by a catch-bond mechanism. These results suggest that pFn polymerization and pFn-dependent catch bonds might also promote vascular interactions for other bacterial pathogens.

Results

***B. burgdorferi*–Endothelial Interactions Under Vascular Shear Stress Depend on Bacterial Recruitment of pFn.** To determine how Fn promotes *B. burgdorferi*-vascular interactions, we studied its mechanistic contributions to bacterial interactions with postconfluent primary human umbilical vein endothelia under physiological shear stress in flow chambers. This flow chamber system recapitulates the major qualitative and quantitative properties of *B. burgdorferi* interactions with dermal PCVs in live mice (7), where the two major types of mobile *B. burgdorferi*-vascular interactions, tethering and dragging, are Fn-dependent (18, 33). Tethering and dragging are distinct initiation steps in the multistep *B. burgdorferi*-vascular interaction cascade and permit bacteria to slow down sufficiently to extravasate from blood vessels during dissemination (7, 18, 19, 33) (Fig. 1*A*). Tethering bacteria are stabilized by tethers anchoring bacteria to endothelia, move at least 50% more slowly under flow than control beads but faster than 100 μm·s^{-1}, and pause briefly and repeatedly as they move over endothelial surfaces (7, 33) (Fig. 1*A*). Dragging bacteria are not stabilized by tethers, and move more slowly than 100 μm·s^{-1} (7, 33) (Fig. 1*A*). Tethering and dragging interactions can be measured by counting numbers of bacteria that pause (tether) or crawl/drag at a speed of less than 100 μm·s^{-1} in a 30 × 100-μm region of interest positioned in unbranched regions of PCVs in vivo (33) or at the center of flow chambers (7).

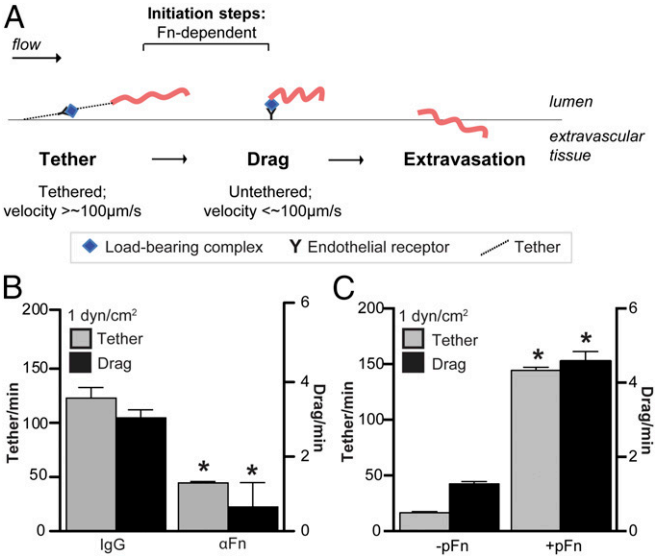

Fig. 1. Dependence of *B. burgdorferi*–endothelial interactions under physiological shear stress on pFn. (*A*) Schematic illustrating initiation steps (tethering, dragging) of the *B. burgdorferi*–endothelial interaction cascade leading to bacterial transmigration across endothelial barriers into extravascular tissues. Tethering bacteria anchor to endothelial surfaces via tethers, pause repeatedly as they move over endothelial surfaces, but move faster than 100 μm·s^{-1}. Dragging bacteria move more slowly (<100 μm·s^{-1}) and are untethered. Both tethering and dragging are Fn-dependent in mouse PCVs (18). There are reduced numbers of *B. burgdorferi* tethering and dragging on primary human endothelial monolayers in flow chambers at typical PCV shear stress (1 dyn/cm^2) following treatment with polyclonal anti-Fn antiserum (*B*) and depletion of pFn from serum in bacterial cultivation medium (*C*). Numbers of tethering and dragging GFP-expressing *B. burgdorferi* (strain GCB966) in the presence of nonspecific IgGs or polyclonal αFn IgGs were measured by manual counting. In *B*, GCB966 was cultivated in the presence of mouse blood before imaging. In *C*, bacteria were cultivated without mouse blood to eliminate all sources of pFn. In *C*, −pFn indicates pFn-depleted growth conditions; for +pFn samples, bacteria grown under pFn-depleted conditions were supplemented with human pFn (+pFn) to the concentration present in blood (0.3 mg/mL) before imaging. Summary values: mean ± SEM. Statistics: two-way ANOVA, Holm–Sidak posttest ($n = 3$ independent bacterial and endothelial cultures per group). *$P < 0.05$ vs. IgG (*B*) or −pFn (*C*) within the same interaction type.

To determine if *B. burgdorferi*–endothelial interactions in flow chambers were Fn-dependent, we treated bacteria with polyclonal IgGs to Fn from rabbit serum (Fig. 1*B*), which is a component of *B. burgdorferi* cultivation medium (34). As observed in mouse dermal PCVs (18), this treatment reduced tethering and dragging at a shear stress typical in PCVs (1 dyn/cm^2; Fig. 1*B*), demonstrating that tethering and dragging interactions with human endothelia under physiological shear stress are also Fn-dependent.

In blood vessels, there are two types of Fn with the potential to support bacterial interactions with vascular surfaces. The first type is the insoluble Fn deposited on the luminal surface of endothelia lining blood vessels (Fig. S1 *A* and *B*). The second type is pFn, which is an abundant constituent of blood (~0.3 mg/mL) and circulates in a soluble, nonadhesive, nonpolymerized state

(11, 12). This pFn is ordinarily a compact, nonadhesive dimer in which most ligand-binding sites are buried. Preservation of the inert, nonadhesive properties of this molecule is important in blood, where constitutive exposure of pFn ligand-binding sites would affect blood flow, thrombosis, and movement and adhesion of circulating cells (11, 21). However, upon activation or force-induced stretching or conformational change induced by certain FnBPs, pFn undergoes a conformational change that exposes ligand-binding sites (11, 12, 26, 27, 35).

The observation that treating *B. burgdorferi* with IgGs against plasma Fn from the serum used to cultivate bacteria inhibited interactions (Fig. 1*B*) suggested that the form of Fn supporting *B. burgdorferi*–endothelial interactions was possibly pFn. To test this hypothesis, we cultivated bacteria in medium depleted of pFn (−pFn) (Fig. S2 *A* and *B*), followed by brief incubation with vehicle (−pFn) or with a physiological concentration of pFn (0.3 mg/mL) purified from human plasma (+pFn) (Fig. S2 *C* and *D*) before perfusion over endothelia (Movies S1–S4). *B. burgdorferi* growth in pFn-depleted and complete media was similar (Fig. S2*B*). Depletion of pFn from bacterial growth medium (Fig. 1*C*) reduced tethering and dragging as effectively as treatment with polyclonal αFn antibody (Fig. 1*B*), implying that the insoluble Fn present on surfaces of endothelial cells themselves was not sufficient to support normal levels of bacterial interaction. Conversely, supplementing bacteria grown in pFn-depleted medium with a physiological concentration of human pFn (0.3 mg/mL) restored interactions (Fig. 1*C*). Interactions were inhibited by treatment with monoclonal antibodies against sites in human Fn involved in Fn fibrillogenesis and interactions with Fn receptors and *B. burgdorferi* adhesins (Fig. S3 and Table S1). Under static (no-flow) conditions, brief coincubation of bacteria with pFn caused rapid lengthwise compression of bacterial cell shape (Fig. S4 *A* and *B*), and BBK32-expressing *B. burgdorferi* also induced pFn fibrillogenesis (Fig. S4*C*) and formation of foci of polymerized pFn at and extending from bacterial cell poles (Fig. S4*D*). We do not know if the polar sites of pFn foci are due to concentration of BBK32 to bacterial cell poles or to other factors, because the subcellular localization patterns of BBK32 have not yet been defined. Thus, bacteria induced widespread conformational changes in pFn that likely exposed ligand-binding sites in this molecule. Collectively, these results indicated that *B. burgdorferi* interactions with human endothelia under physiological shear stress were primarily dependent on bacterial recruitment of pFn.

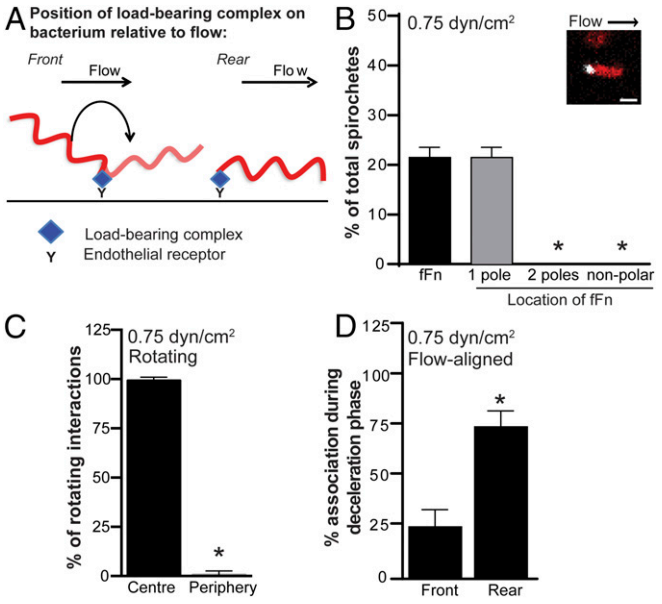

Fig. 2. Localization of polymerized pFn to mechanically loaded adhesion sites on bacteria interacting with endothelia under shear stress. Under physiological shear stress, polymerized pFn localizes to the adhesion sites on bacteria that bear the mechanical load during endothelial interactions. (*A*) Schematic showing the positions on bacteria (front vs. rear, relative to flow direction) that are mechanically loaded when bacteria rotate during endothelial adhesion under flow (front-loaded) or are flow-aligned during adhesion (rear-loaded). *B. burgdorferi* that form adhesions at the front of the bacterial cell rotate/flip under flow. *B. burgdorferi* anchored to endothelia at the rear of bacteria align with flow. (*B*) Polymerized fFn (*Inset*, white) is redistributed exclusively to one cell pole of GCB776 bacteria (*Inset*, red) during endothelial interactions at 0.75 dyn/cm^2 (n = 64 bacteria). *P < 0.05 vs. one pole. (Scale bar: 5 μm.) (*C*) Polymerized fFn localizes exclusively to the center of bacterial cell rotation (load-bearing adhesion site) for *B. burgdorferi* that rotate during endothelial interactions (n = 10 rotating bacteria). *P < 0.05 vs. localization at the center of rotation. (*D*) Polymerized fFn localizes primarily to the rear, load-bearing site when bacteria are decelerating (i.e., when they adhere to endothelia) (n = 17 flow-aligned bacteria). *P < 0.05 vs. localization at front. Summary values in all panels: mean ± 95% confidence interval (CI) (n = 3 independent bacterial and endothelial cultures per experiment). Statistics: two-way ANOVA, Holm–Sidak posttest (*B*) and two-tailed Wilcoxon matched pairs t tests (*C* and *D*).

Polymerized pFn Foci Formed on BBK32-Expressing *B. burgdorferi* Localize to Sites on Bacteria Where Adhesion Complexes Are Mechanically Loaded. Conformational changes associated with pFn polymerization expose many ligand-binding sites that are cryptic in pFn (11). Because BBK32-expressing *B. burgdorferi* formed "caps" of polymerized pFn at and extending from bacterial cell poles (Fig. S4*D*), and because ligand-binding sites in pFn are more likely to be exposed in these foci, we investigated whether pFn foci colocalize with positions on bacteria that contact endothelial surfaces and support mechanical load during interactions (Fig. 2).

B. burgdorferi interacts with endothelia by transferring mechanical load along a series of single adhesion complexes or tightly clustered and coordinated receptor–ligand complexes that dissociate with the kinetics of a single adhesion complex (7). As a result, only one physical site on a bacterium is involved in load-bearing interactions with endothelia at any given time, and that mechanical load is borne by only one receptor–ligand adhesion complex at this site or by a tightly spatially clustered and coordinated group of complexes at this site that behave kinetically as a single complex. On bacteria that flip as they adhere to endothelia under flow, the load-bearing site is located at the cell pole closest to the center of rotation (Fig. 2*A*). On bacteria that are aligned parallel to flow during endothelial interactions, the load-bearing site is typically located at the rear of bacteria that are decelerating (i.e., adhering to endothelia) (Fig. 2*A*). These properties permitted us to determine if foci of polymerized, fluorescent pFn visualized on bacteria by live cell imaging (Fig. 2*B*) colocalized with sites of mechanical loading on these bacteria during endothelial interactions under flow (Fig. 2 *C* and *D*). Although small "specks" of fluorescent pFn were observed at the poles of many bacteria under these conditions, to determine the localization of pFn foci unambiguously with respect to load-bearing adhesion sites, we confined our analysis to bacterial pFn foci with diameters >1 μm, which were observed on ∼20% of bacteria interacting with endothelia under flow (Fig. 2*B*). Experiments were performed at 0.75 dyn/cm^2, a typical shear stress in dermal PCVs (33), because bacteria flip more frequently at this shear stress than at higher shear stresses. These analyses revealed that 99.2% of polymerized pFn foci localized to the load-bearing pole at the center of rotation in flipping bacteria (Fig. 2*C*), and that ∼75% of foci localized to the load-bearing rear of decelerating bacteria that interacted with endothelia in a flow-aligned fashion (Fig. 2*D*). These results implied that polymerized pFn localized nonrandomly to load-bearing adhesion sites on both flipping and flow-aligned bacteria, and was therefore likely part of load-bearing adhesion complexes.

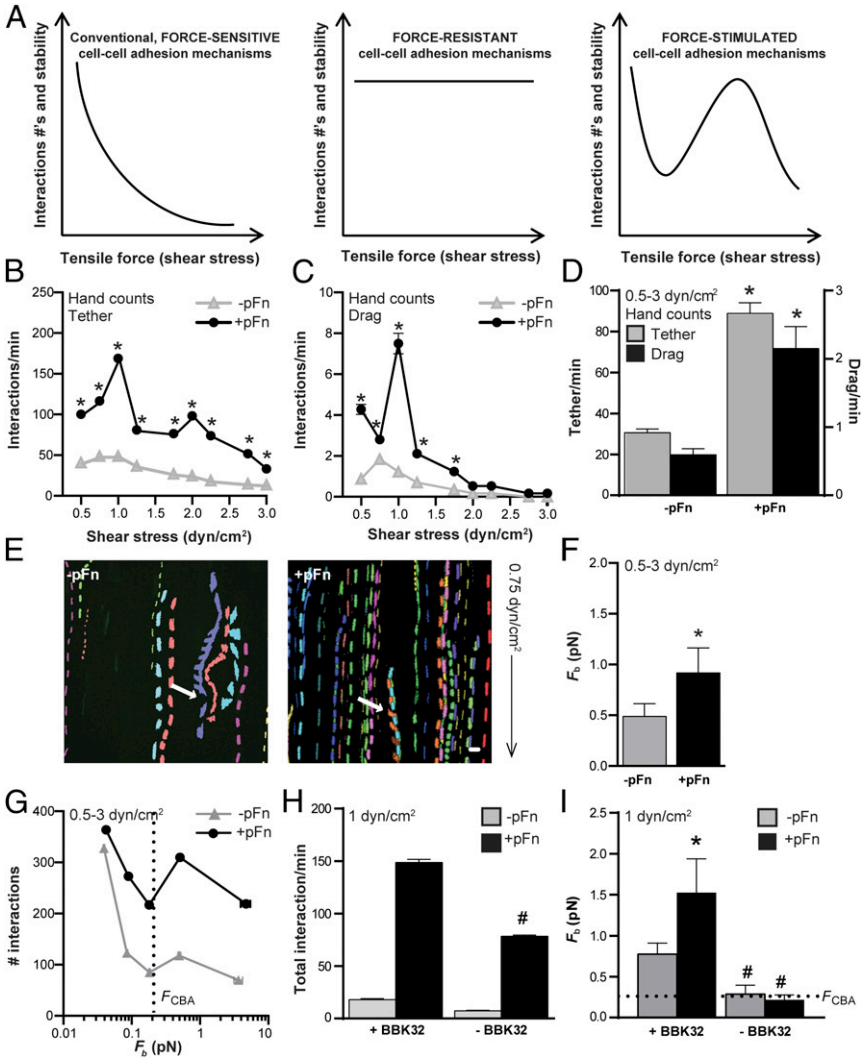

Fig. 3. Effect of pFn on force sustained by load-bearing adhesion complexes. (*A*) Conventional, force-sensitive adhesion complexes fail at exponential rates with linear increases in tensile force such as shear stress (*Left*), whereas force-resistant complexes remain stable (*Center*) and force-stimulated complexes become more stable (longer lived) as tensile force increases above an activation threshold (*Right*) (43). Force-stimulated adhesion complexes eventually fail, but at a higher force than conventional complexes. In vascular environments, where shear stress varies, force-dependent adhesion complex strengthening promotes interaction of circulating cells with vascular surfaces over a broader shear stress range. pFn stimulates mean ± SEM. Tethering (*B*) and dragging (*C*) interactions of BBK32-expressing *B. burgdorferi* (GCB966) with endothelia over a typical PCV shear-stress range (0.5–3 dyn/cm^2) are shown. (*D*) Global mean ± 95% CI interactions for all shear-stress conditions combined. *$P < 0.05$ vs. −pFn within interaction type (two-way ANOVA, Holm–Sidak posttest) (n = 6 independent bacterial cultures per shear-stress condition, for a total of 54 replicates per global mean). (*E–I*) Load-bearing adhesion complexes can withstand greater force in the presence of pFn and the pFn fibrillogenesis-inducing *B. burgdorferi* adhesin BBK32. (*E*) Sample time-lapse projections of interaction trajectories (tracks) for individual bacteria (depicted in different colors) captured by particle tracking over 2 min. White arrows indicate rotating *B. burgdorferi* interacting by one end. The black arrow indicates flow direction. (*F*) Effect of pFn on global mean (±95% CI) F_b for endothelial interactions of BBK32-expressing bacteria shown in *D*. (*G*) Numbers of tracked interactions at indicated mean ± SEM F_b values. Mean ± SEM total interactions per minute (*H*) and mean ± 95% CI bond forces (*I*) at 1 dyn/cm^2 are shown for BBK32-expressing parental bacteria (+BBK32: GCB966) and an isogenic BBK32-deficient strain (–BBK32: GCB971) ($n \geq$ 724 individual interactions analyzed per group). Statistics: two-tailed unpaired Mann–Whitney test (*E–I*) and two-way ANOVA with Holm–Sidak posttests (*H* and *I*). *$P < 0.05$ vs. −pFn within group; #$P < 0.05$ vs. +BBK32 within group.

The pFn Increases Mechanical Load Sustained by Adhesion Complexes Under Vascular Shear Stress. Another way to determine if pFn is part of force-loaded adhesion complexes on *B. burgdorferi* interacting with endothelia is to determine if the force sustained by load-bearing bonds is altered by the presence of pFn (i.e., if pFn affects bond strength). To investigate the effect of pFn on bond strength, we grew *B. burgdorferi* in pFn-depleted conditions, incubated bacteria briefly with vehicle alone (−pFn) or with 0.3 mg/mL pFn (+pFn), and then perfused bacteria over endothelial monolayers at a range of increasing shear stresses found in PCVs (3) (0.5–3 dyn/cm^2; Fig. 3). Interactions were measured from 0.5 to 3 dyn/cm^2 because *B. burgdorferi*–endothelial interactions are progressively stabilized by a force-stimulated catch-bond mechanism as shear stress and force on load-bearing bonds increase over this range, especially from 0.5 to 1 dyn/cm^2 (7). Force-resistant and force-stimulated adhesion mechanisms are particularly important for stabilizing the interaction of circulating cells with endothelial surfaces in the vasculature, where shear stress varies even within one blood vessel, and where small linear changes in shear stress cause conventional, force-sensitive adhesive bonds to fail at an exponential rate (Fig. 3*A*). Both tethering and dragging interactions were more numerous in the presence of pFn, particularly at 1 dyn/cm^2 (Fig. 3 *B–D*), and +pFn interaction numbers increased at 1 dyn/cm^2 (Fig. 3 *B* and

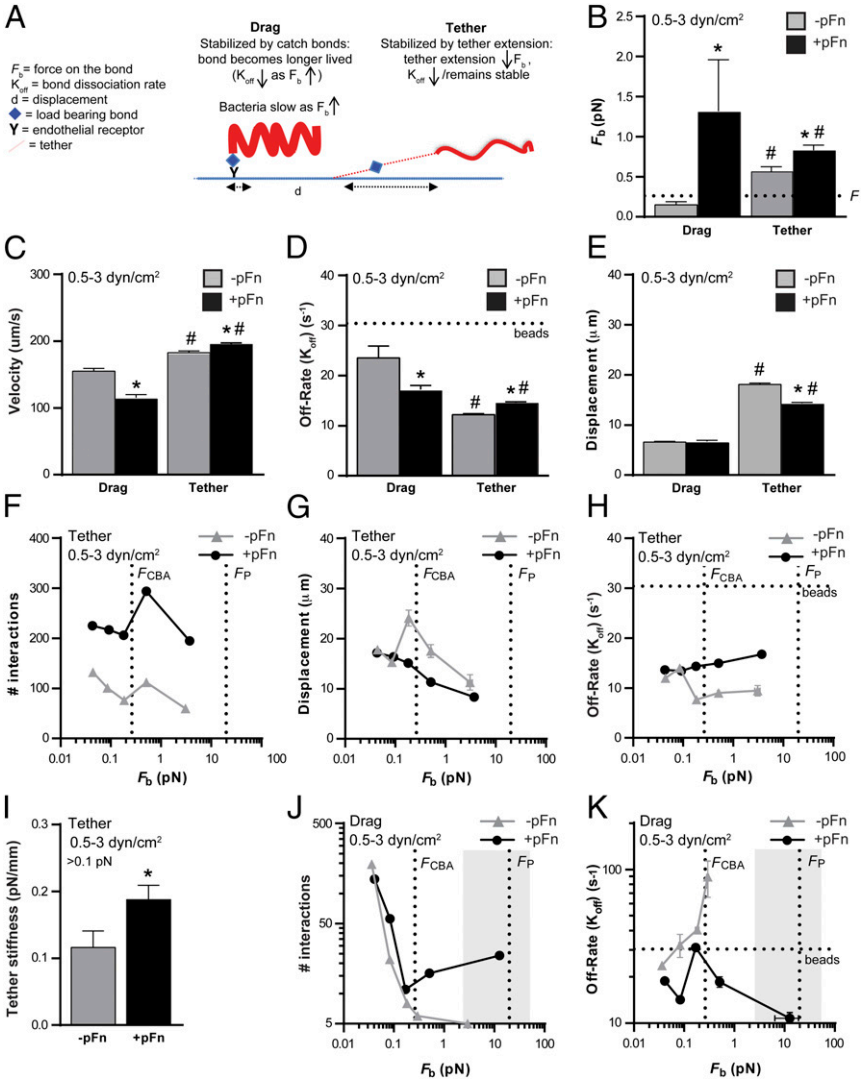

Fig. 4. Stabilization of pFn-dependent *B. burgdorferi*–endothelial interactions by a catch-bond mechanism. Tethered *B. burgdorferi* interactions are more numerous in the presence of pFn at all bond forces. Untethered dragging interactions become longer lived as force increases in the presence of pFn, indicating that pFn strengthens dragging interactions by a catch-bond mechanism. (*A*) Schematic summarizing differences in physical interaction properties of dragging and tethering *B. burgdorferi* (7). *B. burgdorferi* are shaped like a planar sine wave. F_bs and K_{off}s are greatest during dragging, when bacteria project above surfaces in an edge-on conformation (Fig. S5*B*). Tethering bacteria lie flatter against surfaces, and are anchored to endothelia by tethers, which reduce force on load-bearing bonds and increase bond lifetime. Global mean F_bs (*B*), velocity (*C*), K_{off}s (*D*), and displacement (*E*) are shown for tethering and dragging interactions. Tethering interaction numbers (*F*), displacement (*G*), and dissociation rates (*H*) are shown at indicated F_b values. (*I*) Estimated tether stiffness for tethered interactions with bond forces >0.1 pN. Dragging interaction numbers (*J*) and K_{off}s (*K*) are shown at indicated F_bs. Dotted lines: beads (K_{off} for negative control beads; bacterial interactions dissociating as fast or faster than beads are interacting nonspecifically), F_{CBA} (bond force at BBK32-dependent catch bonds are activated) (7), and F_p (bond force at which proteins that are unanchored to cytoskeletal structures are plucked from lipid bilayers; indicates typical maximum bond force for BBK32-dependent interactions). Gray shading in *J* and *K* indicates the catch-bond force regime of Fn–$\alpha_5\beta_1$ complexes, where bond dissociation slows as force increases. The strain used is GCB966 in all panels. Summary values: mean ± 95% CI. Statistics: two-way ANOVA, Holm–Sidak posttest. *$P < 0.05$ vs. −pFn within interaction type; $^{\#}P < 0.05$ vs. drag within group. Independent bacterial and endothelial cultures per group ($n = 6$ per shear stress condition for total of 54 replicates per group; $n \geq 481$ and $n \geq 241$ individual interactions analyzed per group for tethering and dragging, respectively).

C), a shear stress at which catch-bond properties of BBK32-dependent *B. burgdorferi*–endothelial adhesion complexes are activated (7).

To determine if pFn affected the stability and amount of force sustained by load-bearing bonds supporting bacterial-endothelial interactions, we used particle-tracking methods for tracking and measuring the physical properties of individual *B. burgdorferi* interacting with endothelia (Fig. 3*E*) to estimate the average force imposed on load-bearing bonds during interactions (F_b), as described previously (3, 7, 36) and in Fig. S5. All −pFn and +pFn interactions exhibited dissociation kinetics characteristic of single force-loaded adhesion complexes (Fig. S5*D*), implying that although pFn at the load-bearing interaction site on each bacterium was polymerized (Fig. 2), each interaction was nevertheless dependent on loading of a single adhesion bond, or of closely physically clustered and coordinated complexes that behaved as a single bond. These analyses revealed that load-bearing bonds formed in the presence of pFn sustained significantly greater average force than load-bearing bonds formed under −pFn conditions (Fig. 3*F*). Furthermore, at all but the smallest bond forces, +pFn interactions were more abundant than −pFn interactions (Fig. 3*G*). The pFn-dependent stimulation of interactions and increased bond strength at 1 dyn/cm^2 were dependent on the pFn-polymerizing, catch-bond–confer-

ring adhesin BBK32 (Fig. 3 *H* and *I* and Fig. S4*C*). Thus, pFn-dependent interactions sustained more force on the load-bearing bond and promoted interactions at higher bond forces, indicating that pFn contributed to and strengthened load-bearing adhesion complexes.

pFn Promotes Tethering Interactions by Increasing Bond Formation Rates and Stabilizes Dragging by a Catch-Bond Mechanism. Finally, we investigated how pFn promotes the two major types of mobile *B. burgdorferi* interactions with endothelia, tethering and dragging. Tethering and dragging are analogous to the interactions supporting leukocyte rolling on endothelial surfaces, which permit these cells to slow down and extravasate (7) (Fig. 1*A*). Leukocyte rolling on PCV surfaces is stabilized by force-strengthened selectin catch bonds that become longer lived (more stable) as bond force increases, and by elastic membrane-derived tethers associated with load-bearing adhesion complexes that anchor leukocytes to endothelia and stabilize load-bearing bonds by distributing (sharing/reducing) the force imposed on adhesion complexes (3). *B. burgdorferi*–endothelial interactions at PCV shear stress are also stabilized by BBK32-dependent catch-bond properties and by tethers, although the source and composition of tethers are unknown (7). Tethers stabilize *B. burgdorferi*-tethering interactions with endothelia by anchoring bacteria to surfaces and reducing the force imposed on load-bearing bonds, which reduces bond dissociation rates (K_{off}s) and prolongs bond lifetime (7) (Fig. 4*A*). *B. burgdorferi*-dragging interactions with endothelia are untethered, and they are subjected to larger bond forces and dissociate more rapidly than tethered interactions (7) (Fig. 4*A*). Although the bonds supporting dragging interactions are shorter lived than the bonds mediating tethered interactions, the velocity of dragging *B. burgdorferi* is considerably slower, because bacteria move forward in small, inchworm-like steps, whereas tethered interactions displace much further due to elongation of their anchoring tethers (7) (Fig. 4*A*). BBK32-dependent catch bonds are particularly important for increasing the number and stability of *B. burgdorferi*-dragging interactions with endothelia as shear stress increases (7).

We found that although bond forces sustained by tethered bacteria were somewhat greater in the presence of pFn compared with −pFn controls (Fig. 4*B*), tethering bacteria also moved faster (Fig. 4*C*) and bonds dissociated slightly more quickly (Fig. 4*D*) after shorter displacement distances (Fig. 4*E*). These observations suggested that in the presence of pFn, tethered interactions were less stable and that increased numbers of tethering interactions under +pFn conditions (Fig. 3*D*) were possibly due to increased bond formation rates. To test this hypothesis, we examined tethered interaction numbers over a range of bond forces, and found that interaction abundance profiles under −pFn and +pFn conditions were similar and that tethered interactions were consistently more abundant at all bond forces (Fig. 4*F*). These findings suggested that tethered interactions formed more readily in the presence of pFn. Examination of tether extension as a function of bond force also revealed that although force-dependent elongation of tethers at 0.1–0.2 pN was prominent under −pFn conditions, this elongation was absent in the presence of pFn (Fig. 4*G*), and that the slowing of bond dissociation observed for −pFn interactions at the tether extension threshold did not occur for +pFn interactions (Fig. 4*H*). Estimates of the stiffness of tethers anchoring bacteria to endothelia showed that tethers formed in the presence of pFn were also stiffer (Fig. 4*I*). Collectively, these data indicated that tether elongation and associated bond stabilization occurred less readily in the presence of pFn, and that stimulation of tethering interactions by pFn was likely due instead to increased rates of bond formation.

By contrast, in the presence of pFn, dragging interactions moved significantly more slowly (Fig. 4*C*), primarily due to slowing of bond dissociation (Fig. 4*D*), and also sustained much larger bond forces (Fig. 4*B*). Thus, pFn strengthened, stabilized, and slowed untethered interactions. These findings suggested the possibility that pFn promoted untethered interactions by a catch-bond mechanism. Catch bonds are bonds that become longer lived (dissociate more slowly) as bond force increases, and they are important for strengthening Fn–integrin interactions under tension and stabilizing selectin-mediated leukocyte rolling on PCVs under shear stress (4, 13, 14, 16, 17, 37–40), as well as BBK32-dependent *B. burgdorferi*–endothelial interactions under vascular shear-stress conditions (7). BBK32-dependent catch bonds are activated at a slightly higher bond force (~0.25 pN) than the force threshold at which tether elongation occurs (7) (0.1–0.2 pN; Fig. 4*G*). To determine if pFn promoted untethered interactions by a catch-bond mechanism, we examined the abundance (Fig. 4*J*) and stability (Fig. 4*K*) of dragging interactions over a range of bond forces. In the absence of pFn, only tethering interactions (Fig. 4*F*), but not dragging interactions (Fig. 4*J*), were observed at bond forces greater than ~0.2 pN, implying that without pFn, *B. burgdorferi* could not interact with endothelial cells at forces higher than this threshold unless interactions were stabilized by tethers. In the absence of pFn, interaction numbers also decreased exponentially and dissociated at exponentially faster rates, with linear increases in bond force above the BBK32 catch-bond activation threshold (~0.25 pN; Fig. 4 *J* and *K*). Thus, without pFn, interactions exhibited kinetics characteristic of conventional slip bonds, which become less stable under increasing force. However, when pFn was present, dragging interactions exhibited kinetics characteristic of catch bonds at bond forces greater than ~0.2 pN; that is, dragging interaction numbers progressively increased and bonds became progressively longer lived as force increased (Fig. 4 *J* and *K*). Together, these data indicated that *B. burgdorferi* could not interact with endothelial cells at bond forces greater than ~0.2 pN in the absence of pFn unless interactions were stabilized by tethers, and that pFn stabilized untethered interactions above this force threshold by a catch-bond mechanism. The force regime over which +pFn-dependent catch bonds were formed was comparable to the catch-bond force regimes of BBK32 and Fn–$\alpha_5\beta_1$ complexes, as well as leukocyte selectins (4, 7, 13, 16, 17, 37).

Discussion

These results show that *B. burgdorferi* exploits pFn, an abundant constituent of blood, to facilitate bacterial interactions with endothelia under vascular shear stress. pFn increased the shear-stress range of *B. burgdorferi*–endothelial interactions and the force sustained by load-bearing bonds in BBK32-expressing bacteria (Fig. 3), increased the abundance of all bacterial–endothelial interactions (Fig. 3), and stabilized and slowed dragging interactions by a catch-bond mechanism (Fig. 4). These effects may promote *B. burgdorferi* slowing and extravasation over a wider range of shear-stress conditions in the vasculature, and possibly in a wider range of tissues. It is also possible that pFn recruitment may promote endothelial interactions under vascular shear-stress conditions for other bacterial pathogens. Bacterial exploitation of pFn to facilitate endothelial interactions under flow may increase the risk of pathological infection outcomes such as endocarditis, colonization of cardiac and other devices, bacterial dissemination to secondary infection sites, and possibly immune evasion secondary to invasion of endothelial cells themselves (12, 20, 22).

BBK32 binds to the N-terminal fibrillogenesis region of Fn by the same tandem β-zipper mechanism exhibited by FnBPs from genetically distant staphylococcal and streptococcal bacteria, suggesting the possibility that FnBPs from other disseminating

bacterial pathogens that also induce structural rearrangement of pFn (12, 21) have the potential to strengthen and stabilize bacterial-vascular interactions by a catch-bond mechanism. For one of these adhesins, *S. aureus* FnBPA, polymorphisms that increase the frequency and strength of Fn binding are associated with increased risk of infection of cardiac devices in patients (20, 29). It has not yet been determined if, like BBK32, other FnBPs are capable of inducing Fn fibrillogenesis or forming Fn-dependent catch bonds under mechanical force. This hypothesis warrants investigation, because any mechanism that strengthens bacterial–endothelial interactions under vascular shear stress conditions has the potential to facilitate bacterial adhesion to blood vessel surfaces in vascular beds of organs such as the heart and brain, where forces caused by blood flow are stronger than in other tissues. It has also been assumed that the form of Fn targeted by *S. aureus* that adheres to cardiac devices is Fn-deposited on the surfaces of these devices (20). However, our results suggest that bacterial recruitment of soluble pFn in the blood also has the potential to support these interactions, especially at sites without abundant deposits of insoluble Fn. Interestingly, BBK32-like FnBPs from streptococcal and staphylococcal species undergo structural unbinding when Fn fibers are stretched (41). It is unknown if BBK32 detaches from pFn fibrils when they are stretched, a property that could contribute to the faster dissociation of BBK32-dependent tethered interactions in the presence of pFn (Fig. 4).

We have not yet defined the molecular mechanisms by which pFn promotes *B. burgdorferi*–endothelial interactions under vascular shear stress. However, data presented here suggest that pFn likely facilitates interactions in multiple ways. The pFn increased interaction abundance for both BBK32-expressing and *bbk32*-null bacteria (Fig. 3*H*), indicating that even in the absence of BBK32-dependent pFn polymerization and interaction stabilization by catch bonds, pFn promotes *B. burgdorferi*–endothelial interactions under shear stress. This increase in interactions could be because pFn recruitment expands the range of endothelial cell surface molecules (e.g., heparin-sulfated GAGs, integrins, nonintegrin receptors) with which bacteria can interact (11, 21). It is also possible that force-driven Fn polymerization (42) promotes binding of pFn on bacterial surfaces to insoluble Fn deposited on endothelial surfaces. Conformational changes in pFn induced by Fn-binding adhesins, and possibly by forces induced by nonspecific contacts between pFn-coated bacteria and the endothelial glycocalyx/endothelial cells, are almost certainly required for pFn-dependent interactions, because many ligand-binding sites in globular pFn dimers are not exposed until the molecule undergoes conformational change (21).

For BBK32-expressing *B. burgdorferi*, polymerized pFn foci at bacterial cell poles localized nonrandomly and consistently to mechanically loaded adhesion sites on bacteria (Fig. 2), suggesting that polymerized pFn itself and/or conformational changes associated with pFn polymerization played key roles in BBK32-dependent endothelial interactions under flow. It is possible that pFn polymerization exposed cryptic sites in pFn facilitating binding to endothelial surface receptors, and/or directly strengthened and stabilized adhesion complexes after bond formation. Additionally, BBK32-Fn binding not only induces conformational elongation and polymerization of pFn but also structurally stabilizes a large intrinsically disordered region of BBK32 by a high-affinity tandem β-zipper mechanism (25–27). Thus, by stabilizing BBK32 conformation, pFn may improve this adhesin's ability to withstand force. Finally, it is possible that BBK32/pFn-dependent interaction stabilization was not exclusively due to structural stabilization of BBK32–pFn complexes but also resulted from force-stimulated conformational changes and activation of high-affinity–binding sites in endothelial receptors targeted by these complexes (Fig. 5). Because Fn interactions with integrin $\alpha_5\beta_1$ are stabilized by a force-activated catch-bond mechanism and by cyclic

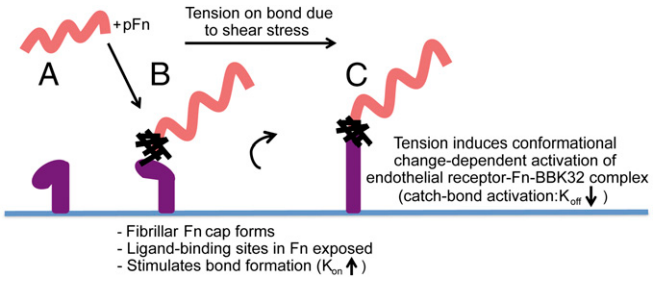

Fig. 5. Proposed model: pFn-dependent mechanisms promoting *B. burgdorferi*–endothelial interactions under shear stress. BBK32-expressing *B. burgdorferi* (*A*) induces pFn conformational changes and polymerization, exposing binding sites for endothelial receptors (possibly integrins) (*B*). The exposure of ligand-binding sites increases interaction numbers by increasing the bond formation rate (K_{on}). (*C*) When the load-bearing adhesion complex is stretched as bacteria are pushed/pulled by shear stress, additional force-induced conformational changes in adhesion complex components (BBK32, pFn, and endothelial receptors) promote formation of a higher affinity, longer lived catch bond.

mechanical reinforcement (13, 14, 16, 17), it is plausible that endothelial receptors themselves also contribute to stabilization of mechanically loaded BBK32–pFn bacterial adhesion complexes. Our preliminary antibody-based mapping of pFn sites mediating interactions suggests that Fn receptors such as $\alpha_5\beta_1$, $\alpha_4\beta_1$, $\alpha_4\beta_7$, and other Fn synergy site-dependent ligands that bind to sequences in Fn regions $FnIII_5$ and synergy site-containing $FnIII_9$ may contribute to interactions; however, because these regions are also involved in Fn fibrillogenesis, we cannot be sure that the effects of antibodies directed against these sites are not also due to disruption of pFn polymerization (Fig. S3). Despite the complexity of the potential molecular mechanisms underlying pFn-dependent *B. burgdorferi*-endothelial interactions, defining these mechanisms will be important for understanding dissemination mechanisms of *B. burgdorferi* and possibly other bacterial pathogens.

Cell–cell interactions in the vasculature depend on mechanically specialized interactions that can overcome shear stress due to blood flow. For disseminating bacteria, the mechanisms supporting these interactions have remained largely undefined for most pathogens. Most disseminating bacterial pathogens have been found to bind Fn, and many of these bacterial pathogens bind to pFn. The results of this study show that the ability to recruit pFn from blood provides a mechanical advantage to *B. burgdorferi* interacting with endothelial surfaces under physiological shear stress, and may thus facilitate bacterial escape from the vasculature and colonization of extravascular tissues. It is possible that similar exploitation of pFn may also prove important for the dissemination mechanisms of other pathogens.

Materials and Methods

Materials and methods for Figs. S1–S5 are discussed in *SI Materials and Methods*.

Ethics Statements. This study conforms to the principles outlined in the most recent policies of The Canadian Council on Animal Care. Animal work was approved by the University of Toronto Animal Care Committee in accordance with institutional guidelines (Protocol 20011501). The authors declare no competing financial or other conflict of interest.

Endothelial Cell Cultivation and Labeling for Live Cell Imaging Flow Chamber Experiments. As described elsewhere (7), all experiments were performed with low-passage primary human umbilical vein endothelial cells pooled from multiple donors (catalog no. CC-2519A; Lonza, Inc.). Endothelial cells (~1.59×10^5 cells) were plated into each channel of an ibiTreat hydrophilic tissue culture-treated Ibidi μ-Slide $VI^{0.4}$ (Ibidi GmbH), grown to 2 d post-confluence, and were labeled with CellMask Deep Red live cell imaging dye (Life Technologies) before imaging.

***B. burgdorferi* Strains, Cultivation, and Preparation for Live Cell Imaging.** Bacterial strains GCB966, GCB776, and GCB971 (Table S2) were grown in Barbour-Stonner-Kelly-II (BSK-II) medium containing 6% heat-inactivated whole or pFn-depleted rabbit serum and 100 μg/mL gentamicin, and were prepared for imaging by washing and resuspension to 1×10^8 cells per milliliter in HBSS as described elsewhere (7, 19). Bacteria used in polyclonal αFn antibody experiments were cultivated in 1% mouse blood, 100 μg/mL gentamicin, 20 μg/mL phosphomycin, 50 μg/mL rifampicin, and 2.5 μg/mL amphotericin for 48 h before preparation for imaging, as described elsewhere (33). Blood was obtained by cardiac puncture with heparinized needles in C57BL/6 mice (Charles River Laboratories) anesthetized with 10 mg/kg xylazine (MTC Pharmaceuticals) and 200 mg/kg ketamine hydrochloride (Rogar/STB). Bacterial cultures that were grown in rabbit serum depleted of pFn were reconstituted with vehicle (saline) or physiological concentrations (0.3 mg/mL) of pFn or HiLyte Fluor 488-labeled pFn (fFn; Cytoskeleton, Inc.) using 1 mg/mL purified pFn stocks, incubated at 4 °C for 1 h, stored on ice, and diluted to 1×10^8 cells per milliliter in HBSS before imaging. All flow chamber experiments were performed with bacteria resuspended in HBSS alone (no added serum), except the experiments reported in Fig. 1*B*, in which heat-inactivated FBS was added to a 10% final concentration. Perfusion of bacteria over endothelial monolayers at 0.5–3 dyn/cm^2 was performed using a syringe pump, as described elsewhere (7). The average length of bacteria following incubation with pFn or vehicle was calculated from all measurements obtained during 1-min time-lapse video-recordings of bacteria adhering to endothelia under static conditions.

Live Cell Imaging Microscopy Conditions. All flow chamber experiments except those experiments reported in Fig. 2 and Fig. S4 were performed as described elsewhere (7) on a Quorum Spinning Disk Confocal microscope (Quorum Technologies, Inc.) equipped with a Zeiss 25×/0.8-N.A. water immersion lens at the Hospital for Sick Children Imaging Facility (Toronto, ON, Canada). Images were acquired at 100% laser power and maximum sensitivity, at 14–15 fps, and at 0.375 μm per pixel, using Volocity software v.6.3.0 (Improvision/PerkinElmer). The experiments reported in Fig. 2 and Fig. S4 were performed by resonant scanner microscopy in a bidirectional resonant scanning mode (8,000 Hz), with an aperture size of 0.95, using a tandem resonant scanner TCS SP8 confocal microscope (Leica) equipped with argon, HeNe, and diode-pumped solid-state (DPSS) lasers; triple dichroic (TD) 488/561/633 excitation beam splitters; hybrid detector (HyD) spectral detectors; and an HCX IRAPO L 25×/0.95-N.A. water immersion objective (Leica). Time courses were acquired at 512 × 512 pixels, 0.61 μm per pixel, and ∼15 fps, with line averaging of 2. Excitation/emission wavelengths for fFn were 488 (argon laser 100% power) and 498–550 nm, respectively, and gain was set to 23. Excitation/emission wavelengths for Tomato-expressing *B. burgdorferi* were 561 (DPSS laser, 37.45% power) and 571–610 nm, respectively, with gain set to 10. Image acquisition software was Leica AF version 3.0.0, build 8139, and offline analysis was performed using Leica LAS software. Cells were kept warm during imaging with an infrared heat lamp.

Localization of Polymerized fFn on Live *B. burgdorferi*. The percentage of Tomato-expressing *B. burgdorferi* associated with polymerized fFn (where fFn colocalized and moved with bacteria) in time-lapse video-recordings was counted manually, after coincubating bacteria grown under Fn-depleted conditions with 0.3 mg/mL fFn for 1 h at 4 °C. Bacteria for which the presence, absence, and/or localization of fFn could not be determined unambiguously were excluded from analysis. The following localization parameters were manually scored for *B. burgdorferi*-associated fFn at each time point in time-lapse series: unipolar, bipolar, or nonpolar localization; localization to the front or rear of bacteria relative to flow direction for bacteria aligned with flow during interactions; and localization to the center or periphery of rotation for bacteria that rotated or flipped as they moved. To determine whether bacteria were accelerating or decelerating, we scored whether bacteria at each time point were moving faster or slower than at immediately preceding time points, based on tracking-based velocity measurements.

Quantitative Image Analysis and Measurement of Biophysical Interaction Properties. All images used for quantification were acquired under identical imaging conditions (identical among all groups reported in each experiment), and no postacquisition image processing was performed before quantification. Tethering and dragging interactions were manually counted in a 30 × 100-μm region of interest at the center of the field of view, as described elsewhere (7). As described in detail recently, bacterial–endothelial interaction trajectories were tracked offline using centroid-based particle-tracking methods and Volocity software. Tracks used for subsequent analyses were tracks with velocities <300 μm·s^{-1}, which is <40% of the velocity of control beads in PCVs and flow chambers at similar shear-stress conditions (7, 33). As described in detail recently (7), the duration (lifetime), velocity, and displacement of bacterial interactions during adhesion to endothelia (deceleration phase of interactions), as well as changes in bacterial length and diameter during interactions, were measured for interaction tracks obtained from time courses and used to estimate interaction K_{off}s and the force sustained by load-bearing bonds (F_b). As described elsewhere (7, 36, 37), to estimate interaction K_{off} rates, natural logarithms of frequencies of individual adhesion events with lifetimes $\geq t$ (lifetime duration) were plotted against t, and curves were fit with straight lines by nonlinear regression in GraphPad Prism (GraphPad Software). R^2 values for lines were ≥0.9. Goodness of fit was evaluated by runs tests ($P > 0.05$ for all runs tests, indicating nonsignificant deviation from linearity). Interaction K_{off}s were estimated from negative slopes of lines. F_b estimates were obtained by methods described in detail previously (3, 7). Schematic illustrations of these methods and associated calculations are also provided in Fig. S5 *A* and *B*. F_b was calculated from $F_b = F_s/\cos\theta$, where force due to flow (F_s) = 31.97 $\tau_w r^2$, τ_w is wall shear stress, r is the radius of bacteria projecting above endothelial surfaces, and θ is bond angle. Bond angle (θ) was calculated from $\cos\theta = l/R$, where l = bacterial displacement during deceleration.

Statistical Analysis. All statistical analysis was performed in GraphPad Prism. Specific statistical tests used are described in the figure legends. Statistical comparisons of differences in slopes for K_{off} calculations were compared using extra sum-of-square F tests.

ACKNOWLEDGMENTS. We thank the T.J.M laboratory members and J. Skare for review of the manuscript. We thank the Department of Comparative Medicine and Sick Kids Imaging Facility for technical support. We thank A. Eshghi and N. Zlotnikov for assistance with manuscript preparation. We thank G. Chaconas for providing bacterial strains. T.J.M was supported by funding from Canadian Institutes of Health Research (CIHR) Grants MOP-11959 and ICS-12398, Natural Sciences and Engineering Research Council (NSERC) Grant RGPIN 401938-11, Collaborative Health Research Projects (CHRP) Grants CIHR/NSERC 494968 and 494982, the Banting Research Foundation, and Canada Foundation for Innovation/Ontario Research Fund (CFI/ORF) Grant 27881. B.H. was supported by funding from CIHR Grants 210820, 286920, and 286720; CHRP Grants CIHR/NSERC 1004005 and 413783; and CFI/ORF Grant 26653. A.F.N. and R.E. were supported by a graduate scholarship from the University of Toronto and a Harron Fellowship. R.E. was supported by an Ontario Graduate Scholarship and a Faculty of Dentistry Undergraduate Summer Studentship.

1. Lemichez E, Lecuit M, Nassif X, Bourdoulous S (2010) Breaking the wall: Targeting of the endothelium by pathogenic bacteria. *Nat Rev Microbiol* 8:93–104.
2. Cahill TJ, Prendergast BD (2016) Infective endocarditis. *Lancet* 387:882–893.
3. Sundd P, Pospieszalska MK, Cheung LS-L, Konstantopoulos K, Ley K (2011) Biomechanics of leukocyte rolling. *Biorheology* 48:1–35.
4. Marshall BT, et al. (2003) Direct observation of catch bonds involving cell-adhesion molecules. *Nature* 423:190–193.
5. Beaussart A, et al. (2014) Nanoscale adhesion forces of *Pseudomonas aeruginosa* type IV Pili. *ACS Nano* 8:10723–10733.
6. Persat A, et al. (2015) The mechanical world of bacteria. *Cell* 161:988–997.
7. Ebady R, et al. (2016) Biomechanics of *Borrelia burgdorferi* vascular interactions. *Cell Reports* 16:2593–2604.
8. Bernard SC, et al. (2014) Pathogenic Neisseria meningitidis utilizes CD147 for vascular colonization. *Nat Med* 20:725–731.
9. Pappelbaum KI, et al. (2013) Ultralarge von Willebrand factor fibers mediate luminal *Staphylococcus aureus* adhesion to an intact endothelial cell layer under shear stress. *Circulation* 128:50–59.
10. Claes J, et al. (2014) Adhesion of *Staphylococcus aureus* to the vessel wall under flow is mediated by von Willebrand factor-binding protein. *Blood* 124:1669–1676.
11. Singh P, Carraher C, Schwarzbauer JE (2010) Assembly of fibronectin extracellular matrix. *Annu Rev Cell Dev Biol* 26:397–419.
12. Henderson B, Nair S, Pallas J, Williams MA (2011) Fibronectin: A multidomain host adhesin targeted by bacterial fibronectin-binding proteins. *FEMS Microbiol Rev* 35: 147–200.
13. Kong F, García AJ, Mould AP, Humphries MJ, Zhu C (2009) Demonstration of catch bonds between an integrin and its ligand. *J Cell Biol* 185:1275–1284.
14. Chakrabarti S, Hinczewski M, Thirumalai D (2014) Plasticity of hydrogen bond networks regulates mechanochemistry of cell adhesion complexes. *Proc Natl Acad Sci USA* 111:9048–9053.
15. Sampaio ALF, et al. (2010) Inflammation-dependent alpha 5 beta 1 (very late antigen-5) expression on leukocytes reveals a functional role for this integrin in acute peritonitis. *J Leukoc Biol* 87:877–884.
16. Friedland JC, Lee MH, Boettiger D (2009) Mechanically activated integrin switch controls $\alpha_5\beta_1$ function. *Science* 323:642–644.

17. Kong F, et al. (2013) Cyclic mechanical reinforcement of integrin-ligand interactions. *Mol Cell* 49:1060–1068.
18. Norman MU, et al. (2008) Molecular mechanisms involved in vascular interactions of the Lyme disease pathogen in a living host. *PLoS Pathog* 4:e1000169.
19. Moriarty TJ, et al. (2012) Vascular binding of a pathogen under shear force through mechanistically distinct sequential interactions with host macromolecules. *Mol Microbiol* 86:1116–1131.
20. Messina JA, Thaden JT, Sharma-Kuinkel BK, Fowler VG, Jr (2016) Impact of bacterial and human genetic variation on *Staphylococcus aureus* infections. *PLoS Pathog* 12: e1005330.
21. Maurer LM, Ma W, Mosher DF (2015) Dynamic structure of plasma fibronectin. *Crit Rev Biochem Mol Biol* 51:213–227.
22. Hymes JP, Klaenhammer TR (2016) Stuck in the middle: Fibronectin-binding proteins in gram-positive bacteria. *Front Microbiol* 7:1504.
23. Stoffels JMJ, Zhao C, Baron W (2013) Fibronectin in tissue regeneration: Timely disassembly of the scaffold is necessary to complete the build. *Cell Mol Life Sci* 70: 4243–4253.
24. Wang Y, Ni H (2016) Fibronectin maintains the balance between hemostasis and thrombosis. *Cell Mol Life Sci* 73:3265–3277.
25. Raibaud S, et al. (2005) *Borrelia burgdorferi* binds fibronectin through a tandem beta-zipper, a common mechanism of fibronectin binding in staphylococci, streptococci, and spirochetes. *J Biol Chem* 280:18803–18809.
26. Harris G, Ma W, Maurer LM, Potts JR, Mosher DF (2014) *Borrelia burgdorferi* protein BBK32 binds to soluble fibronectin via the N-terminal 70-kDa region, causing fibronectin to undergo conformational extension. *J Biol Chem* 289:22490–22499.
27. Prabhakaran S, Liang X, Skare JT, Potts JR, Höök M (2009) A novel fibronectin binding motif in MSCRAMMs targets F3 modules. *PLoS One* 4:e5412.
28. Morla A, Zhang Z, Ruoslahti E (1994) Superfibronectin is a functionally distinct form of fibronectin. *Nature* 367:193–196.
29. Lower SK, et al. (2011) Polymorphisms in fibronectin binding protein A of *Staphylococcus aureus* are associated with infection of cardiovascular devices. *Proc Natl Acad Sci USA* 108:18372–18377.
30. Sullan RMA, Li JK, Crowley PJ, Brady LJ, Dufrêne YF (2015) Binding forces of *Streptococcus mutans* P1 adhesin. *ACS Nano* 9:1448–1460.
31. Müller NF, et al. (2011) Trimeric autotransporter adhesin-dependent adherence of *Bartonella henselae*, *Bartonella quintana*, and *Yersinia enterocolitica* to matrix components and endothelial cells under static and dynamic flow conditions. *Infect Immun* 79:2544–2553.
32. Bustanji Y, et al. (2003) Dynamics of the interaction between a fibronectin molecule and a living bacterium under mechanical force. *Proc Natl Acad Sci USA* 100: 13292–13297.
33. Moriarty TJ, et al. (2008) Real-time high resolution 3D imaging of the lyme disease spirochete adhering to and escaping from the vasculature of a living host. *PLoS Pathog* 4:e1000090.
34. Barbour AG (1984) Isolation and cultivation of Lyme disease spirochetes. *Yale J Biol Med* 57:521–525.
35. Marjenberg ZR, et al. (2011) Cooperative binding and activation of fibronectin by a bacterial surface protein. *J Biol Chem* 286:1884–1894.
36. Alon R, Hammer DA, Springer TA (1995) Lifetime of the P-selectin-carbohydrate bond and its response to tensile force in hydrodynamic flow. *Nature* 374:539–542.
37. Sarangapani KK, et al. (2004) Low force decelerates L-selectin dissociation from P-selectin glycoprotein ligand-1 and endoglycan. *J Biol Chem* 279:2291–2298.
38. Le Trong I, et al. (2010) Structural basis for mechanical force regulation of the adhesin FimH via finger trap-like beta sheet twisting. *Cell* 141:645–655.
39. Sauer MM, et al. (2016) Catch-bond mechanism of the bacterial adhesin FimH. *Nat Commun* 7:10738.
40. Thomas WE, Trintchina E, Forero M, Vogel V, Sokurenko EV (2002) Bacterial adhesion to target cells enhanced by shear force. *Cell* 109:913–923.
41. Chabria M, Hertig S, Smith ML, Vogel V (2010) Stretching fibronectin fibres disrupts binding of bacterial adhesins by physically destroying an epitope. *Nat Commun* 1:135.
42. Baneyx G, Baugh L, Vogel V (2002) Fibronectin extension and unfolding within cell matrix fibrils controlled by cytoskeletal tension. *Proc Natl Acad Sci USA* 99:5139–5143.
43. Sokurenko EV, Vogel V, Thomas WE (2008) Catch-bond mechanism of force-enhanced adhesion: Counterintuitive, elusive, but ... widespread? *Cell Host Microbe* 4:314–323.
44. Retta SF, Ferraris P, Tarone G (1999) Purification of fibronectin from human plasma. *Methods Mol Biol* 96:119–124.
45. Probert WS, Johnson BJ (1998) Identification of a 47 kDa fibronectin-binding protein expressed by *Borrelia burgdorferi* isolate B31. *Mol Microbiol* 30:1003–1015.
46. Pankov R, Momchilova A (2009) Fluorescent labeling techniques for investigation of fibronectin fibrillogenesis (labeling fibronectin fibrillogenesis). *Methods Mol Biol* 522: 261–274.
47. Pankov R, et al. (2000) Integrin dynamics and matrix assembly: tensin-dependent translocation of alpha(5)beta(1) integrins promotes early fibronectin fibrillogenesis. *J Cell Biol* 148:1075–1090.
48. Brissette CA, Bykowski T, Cooley AE, Bowman A, Stevenson B (2009) *Borrelia burgdorferi* RevA antigen binds host fibronectin. *Infect Immun* 77:2802–2812.
49. Früh SM, Schoen I, Ries J, Vogel V (2015) Molecular architecture of native fibronectin fibrils. *Nat Commun* 6:7275.
50. Moyano JV, et al. (1997) Fibronectin type III5 repeat contains a novel cell adhesion sequence, KLDAPT, which binds activated alpha4beta1 and alpha4beta7 integrins. *J Biol Chem* 272:24832–24836.
51. Barczyk M, Carracedo S, Gullberg D (2010) Integrins. *Cell Tissue Res* 339:269–280.
52. Ruoslahti E (1996) RGD and other recognition sequences for integrins. *Annu Rev Cell Dev Biol* 12:697–715.
53. Goldstein SF, Buttle KF, Charon NW (1996) Structural analysis of the *Leptospiraceae* and *Borrelia burgdorferi* by high-voltage electron microscopy. *J Bacteriol* 178: 6539–6545.
54. Grant MB, et al. (1998) Matrix metalloproteinase expression in human retinal microvascular cells. *Diabetes* 47:1311–1317.
55. An B, et al. (2014) Definition of the native and denatured type II collagen binding site for fibronectin using a recombinant collagen system. *J Biol Chem* 289:4941–4951.
56. Peters JH, et al. (2001) Preferential recognition of a fragment species of osteoarthritic synovial fluid fibronectin by antibodies to the alternatively spliced EIIIA segment. *Arthritis Rheum* 44:2572–2585.
57. Schor SL, et al. (2003) Migration-stimulating factor: A genetically truncated onco-fetal fibronectin isoform expressed by carcinoma and tumor-associated stromal cells. *Cancer Res* 63:8827–8836.
58. Mosher DF (1980) Fibronectin. *Prog Hemost Thromb* 5:111–151.
59. Katayama M, et al. (1989) Isolation and characterization of two monoclonal antibodies that recognize remote epitopes on the cell-binding domain of human fibronectin. *Exp Cell Res* 185:229–236.
60. Hubbard B, Buczek-Thomas JA, Nugent MA, Smith ML (2014) Heparin-dependent regulation of fibronectin matrix conformation. *Matrix Biol* 34:124–131.
61. Underwood PA, Dalton BA, Steele JG, Bennett FA, Strike P (1992) Anti-fibronectin antibodies that modify heparin binding and cell adhesion: Evidence for a new cell binding site in the heparin binding region. *J Cell Sci* 102:833–845.
62. Pierschbacher MD, Ruoslahti E (1984) Cell attachment activity of fibronectin can be duplicated by small synthetic fragments of the molecule. *Nature* 309:30–33.
63. Wu J, Weening EH, Faske JB, Höök M, Skare JT (2011) Invasion of eukaryotic cells by *Borrelia burgdorferi* requires $\beta(_1)$ integrins and Src kinase activity. *Infect Immun* 79: 1338–1348.
64. Lee W-Y, et al. (2010) An intravascular immune response to *Borrelia burgdorferi* involves Kupffer cells and *i*NKT cells. *Nat Immunol* 11:295–302.